



Physical, Mechanical, and Tribological Properties of Industrial Waste Fly Ash Reinforced AA5083 Composites Fabricated by Stir Casting Process

Swati Gangwar^{1,2} · Ranjeet Kumar Singh¹ · Prabhat Chand Yadav³ · Sandeep Sahu^{3,4,5}

Received: 5 December 2020 / Revised: 22 June 2021 / Accepted: 30 June 2021 / Published online: 9 July 2021
© The Author(s), under exclusive licence to Springer Nature Switzerland AG 2021

Abstract

Reinforcement of second phase particle in metal/alloy to develop metal matrix composite is a standard practice to enhance various properties required for commercial applications. In this work, an industrial waste, fly ash, has been used as reinforcement in aluminum alloy AA5083 to improve its physical, mechanical, and tribological properties. The metal matrix composites were fabricated using high temperature vacuum stir casting technique with varying fraction of fly ash (viz. 0, 4, and 8 wt.%). Reinforcement of fly ash in Al alloy improved its hardness from ~ 50 BHN (for initial alloy) to ~ 70 BHN for 8 wt.% fly ash. Meanwhile, impact strength indicated a reverse trend in comparison to that of hardness, with a marginal change in values from 258 to 248 J. Wear behavior of fabricated composites was investigated against EN31 hardened steel disc at different process parameters, viz. fly ash content, sliding velocity, and normal load. Worn surface of samples were examined under scanning electron microscope to find the wear mechanism. It showed severe abrasive grooves along with brittle fracture for lower fraction of fly ash (i.e., 0 and 4 wt.%), while mild abrasion followed by fragmentation of protective tribolayer was observed for the larger fraction of fly ash (i.e., 8 wt.%). The optimum condition among various process parameters for minimum sliding wear was obtained by Taguchi design of experiments. The minimum wear rate was obtained for 8 wt.% fly ash reinforced composite at sliding velocity 1.047 m/s and normal load 15 N.

Keywords Metal matrix composite · Fly ash · Mechanical properties · Tribological properties · Taguchi design of experiments

1 Introduction

In the current scenario of globalization, the development of advanced materials has become a necessity for industrial and structural applications. Light weight structures and low cost are the primary requirements for their commercial

applications. In automotive and aerospace sectors, light weight structures help in reducing fuel consumption and emissions [1]. Among various alloys, aluminum alloys are found to be light weighted and cost-effective. These are used widely in automotive and aerospace structures for components like pistons, brake rotors, engine blocks, bearings,

✉ Swati Gangwar
sgme@mmmut.ac.in
Ranjeet Kumar Singh
ranjeet355@gmail.com
Prabhat Chand Yadav
yadav@iitk.ac.in
Sandeep Sahu
ssandy@iitk.ac.in

¹ Department of Mechanical Engineering, Madan Mohan Malaviya University of Technology, Gorakhpur 273016, India

² Department of Mechanical Engineering, Netaji Subhas University of Technology, New Delhi 110078, India

³ Department of Materials Science and Engineering, Indian Institute of Technology Kanpur, Kanpur 208016, India

⁴ Directorate of Nanomaterials, Defence Materials and Stores Research and Development Establishment, Defence Research and Development Organisation, Kanpur 208013, India

⁵ Department of Mechanical Engineering, University of Southampton, Highfield Campus, Southampton SO17 1BJ, UK

owing to their high specific strength, specific stiffness, and thermal conductivity. However, aluminum alloys demonstrate poor tribological properties when applied under hostile environments. This led to the development of aluminum metal matrix composites (MMCs) reinforced with second phase, leading to better physical, mechanical, and tribological properties suitable for their applications in automotive, aerospace, and many other sectors [2, 3]. Continuous fiber reinforced aluminum MMCs are very costly to manufacture. Also, secondary metal forming operations like extrusion, rolling, forging are not feasible on these MMCs, which hinder their use in numerous applications. Hence, particulate reinforcement composites are preferred over continuous fiber reinforcement composites as they allow easy fabrication of MMCs with almost isotropic properties, have low cost, and allow secondary metal forming operations [4].

Hard ceramic particulates like SiO_2 , Al_2O_3 , SiC , B_4C , TiC , and ZrB_2 can improve the properties of Al alloys, however, also lead to an increase in the cost of the composite. A high cost of MMCs is one of the primary reasons restricting their extensive applications. Utilization of suitable industrial waste as reinforcement can reduce their cost. Fly ash is one such kind of industrial waste, produced in large quantities (~40%) in thermal power plants during the combustion of coal and has abundant availability all over the world [5]. Also, fly ash contains traces of toxic elements like Pb, Cd, Hg, U, Th, and therefore, their improper disposal is considered hazardous to human health, soil properties, and environment [6–8]. Hence, utilization of fly ash as reinforcement for the fabrication of metal matrix composite can also reduce environmental pollution. Low density of fly ash leads to light weight but high strength to weight ratio of MMCs in comparison to that of the base alloy. In addition, fly ash makes a better bonding with the matrix. These advantages of fly ash have motivated researchers to develop different kinds of fly ash reinforced Al MMCs and evaluate physical and mechanical properties in recent years [9–14].

Anilkumar et al. [9] synthesized AA6061-based composite reinforced with 10, 15, and 20 wt.% of fly ash having different particle sizes by stir casting route. They found that the hardness, compressive strength, and ultimate tensile strength (UTS) of the composites decreased with an increase in the particle size of the fly ash reinforcement, while an increase in the fly ash content increased these mechanical properties. In a similar work, Selvam et al. [15] reinforced AA6061 alloy with 4, 8, and 12 wt.% of fly ash by compocasting and found an improvement in the microhardness and UTS of the fabricated composites on the incorporation of fly ash. Rohatgi et al. [10] incorporated up to 20–65% volume fractions of fly ash cenospheres into the A356 aluminum alloy matrix using pressure infiltration technique and found that compressive strength, plateau stress, and modulus

of elasticity of the composites increased with an increase in the fly ash content. Juang et al. [11] utilized stir casting and multipath friction stir processing (MP-FSP) to synthesize aluminum alloy ADC6 reinforced with 5 wt.% fly ash. They observed a significant refinement in grain size of the composite by MP-FSP, and consequently, improvement in mechanical properties.

Since reinforcement plays a vital role in the fabrication of composites, therefore, size and distribution of reinforcement largely affects the properties of composites, as suggested by El-Khair et al. [16] Proper mixing of reinforcement with the matrix is pertinent for getting the better performance of materials. Stir casting is an attractive synthesis method for the fabrication of aluminum alloy matrix composites owing to its simplicity, cost-effectiveness, low porosity in the cast product, ability to uniformly distribute the reinforcements, and applicability to mass production of materials. Investigation of wettability of filler materials with matrix in composite was studied by Patil et al. [17] They observed improvement in tensile strength of composite with an increase in fly ash content up to 15 wt.%, followed by a decrease in strength due to poor wettability of the filler particle with the matrix. These literature works indicate that fly ash as reinforcement in metal matrix composites enhances its mechanical properties.

Apart from mechanical properties, investigation of the tribological properties of fabricated composites is desired to understand their suitability for tribological applications. Ramachandra and Radhakrishna [18] fabricated Al-12 wt% Si alloy-based composite reinforced with 5, 10, and 15 wt.% fly ash by liquid metallurgy route and investigated its wear and friction characteristics. They observed an improvement in wear resistance of the fabricated composite with an increase in fly ash content, however, the wear resistance decreased with an increase in track velocity and normal load. The wear of fly ash reinforced composite happened because of micro-cutting, delamination, thermal softening, and oxidation. Sudarshan and Surappa [12, 19] synthesized A356 Al alloy composites containing 6 and 12 vol.% of fly ash particles and studied its dry sliding wear in the load range 20–80 N at a constant sliding velocity of 1 m/s. They observed better wear resistance in fabricated composites compared to that of unreinforced alloy. Prasat and Subramanian [20] used the stir casting method to synthesize AlSi10Mg/fly ash/graphite hybrid composite and characterized its wear behavior using the pin-on-disc machine by varying the load and fly ash content. They observed a decrease in the coefficient of friction (COF) and wear rate of the fabricated composites in comparison to that of the base metal alloy and Al-graphite composite. Uthaya Kumar et al. [21] fabricated the fly ash filled composite material by stir casting method to investigate its wear behavior and found

retention of wear resistance at lower load without significant wear at higher sliding speed. Dinaharan et al. [22] fabricated AA6061/(0, 6, 12, and 18 vol.%) fly ash composites using friction stir processing method and observed an improvement in wear resistance with an increase in the fly ash content. Also, the increase in fly ash content changed the wear mechanism from adhesion to abrasive.

An extensive literature survey on aluminum metal matrix composites reveals fly ash as reinforcement leads better mechanical properties, but several aspects of wear data on aluminum-fly ash metal matrix composites for tribological applications are limited. Wear leads to a gradual degradation of materials with time, causing an untimely collapse of the material. Hence, the objective of the present research is to explore the use of fly ash as a low-cost reinforcement in developing aluminum alloy AA5083-based composites with improved physical, mechanical as well as tribological properties. As the present research deals with numerous process parameters, Taguchi method has been adopted as a design tool to optimize the outcomes in terms of multiple input variables and responses. These findings are expected to contribute to the development of lightweight, low cost, and environment-friendly aluminum products.

2 Materials and Methods

2.1 Matrix Material

Aluminum alloy AA5083 was selected as a matrix material to fabricate the composite. AA5083 alloy has excellent formability, low density, high strength, good corrosion resistance, and weldability. Owing to these properties, AA5083 alloy is used extensively in marine, aerospace, and other transportation applications [23]. The chemical composition of AA5083 alloy (in wt.%) was 4.9 Mg, 0.4 Mn, 0.4 Fe, 0.4 Si, 0.25 Cr, 0.25 Zn, 0.15 Ti, and the rest as Al.

2.2 Reinforcing Material

Fly ash produced by the combustion of coal in a thermal power plant was used as reinforcing material. The composition of the constituent of fly ash was obtained from National Thermal Power Corporation (NTPC), Badarpur, Delhi, India, which is given in Table 1. The morphology of fly ash obtained from the thermal power plant was spherical, as shown in Fig. 1. Fly ash was used as a reinforcing material

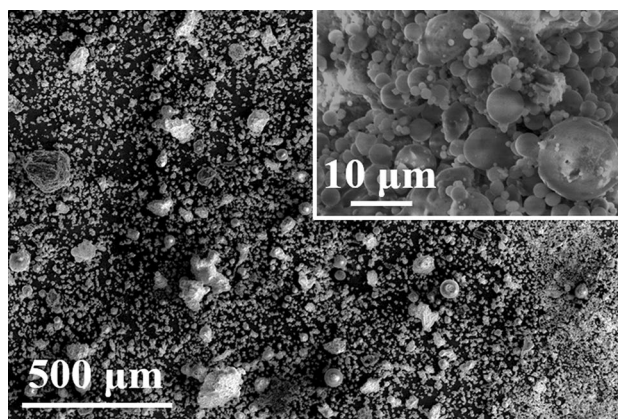


Fig. 1 Morphology of reinforcing material (fly ash) used in AA5083 alloy-based composite

to fabricate composites due to its better properties, viz. low density, low thermal conductivity, and high electrical resistivity. Fly ash, also known as dry ash, has density 2.17 g/cm^3 . Low density and low cost fly ash produces light weight and low-cost metal matrix composites.

2.3 Fabrication of AA5083/Fly Ash Metal Matrix Composite

Aluminum alloy AA5083-based composite was fabricated using high temperature vacuum stir casting technique with varying fractions of fly ash, viz. 0, 4, and 8 wt.%. Stir casting method was used due to its cost-effectiveness, simplicity, and ability to uniformly distribute the reinforcements in the matrix [24]. Here, blend of AA5083 aluminum alloy (in the molten state, at $750 \text{ }^\circ\text{C}$) and dispersed phase (fly ash) was mixed properly using centrifugal stirring for $\sim 5 \text{ min}$. Then, this mixture was poured into a permanent mold and allowed to cool up to room temperature. After getting the solidified composite, specimens were sectioned for further characterization.

2.4 Physical, Mechanical, and Tribological Characterization

2.4.1 Void Content and Density Evaluation

Since the fabrication of composite in the present study was done using stir casting technique, so, there might be chances of trapping of undissolved gases, which may lead to the formation of voids. Therefore, the determination of

Table 1 Composition of fly ash used in the current work

Compound	SiO ₂	Al ₂ O ₃	FeO	CuO	CaO	TiO ₂	MgO	K ₂ O
Composition (Wt. %)	51.43	29.65	5.39	4.86	2.82	2.54	1.73	1.58

void contents is pertinent to evaluate the mechanical and tribological properties of the fabricated composite. The void content of the fabricated composites was evaluated using the following equation [25]:

$$\text{Void content (\%)} = \frac{\rho_t - \rho_e}{\rho_t} \quad (1)$$

where ρ_t is the theoretical density and ρ_e is the experimental density.

The theoretical density was obtained using the rule of mixture according to Eq. (2), proposed by Agarwal and Broutman [26]. Actual density was calculated using Archimedes' principle by measuring the weight of the composite, first in the air and then in water.

$$\text{Theoretical density } (\rho_t) = \frac{1}{\left(\frac{w(m)}{\rho(m)} + \frac{w(p)}{\rho(p)}\right)} \quad (2)$$

where $w(p)$ and $\rho(p)$ are weight fraction and density of particulate material, respectively. $w(m)$ and $\rho(m)$ are weight fraction and density of the matrix material, respectively.

2.4.2 Hardness Test

Hardness test on fabricated composite was conducted using Brinell hardness tester, having the ball indenter of diameter 2.5 mm. Load applied on the specimen was 31.5 Kgf for 10 s dwell time. Brinell hardness number (BHN) was measured using the following equation:

$$\text{BHN} = \frac{2P}{\pi D \left(D - \sqrt{D^2 - d^2} \right)} \quad (3)$$

where P is the load applied on the specimen in Kgf, D is the ball diameter in mm, and d is indent diameter obtained on the specimen in mm.

2.4.3 Impact Test

Impact strength of a material implies its ability to withstand a suddenly applied load. Since composite material fabricated in the present study was intended for use in automotive and aerospace applications where sudden load might be experienced, impact strength was investigated using Charpy test. For conducting Charpy test, the centered notch specimen was placed as simply supported beam, and impact load was applied on the center behind the notch. The standard specimen with V-shape notch, having notch angle of 45° was prepared, where notch was placed on the tension side of the specimen.

2.4.4 Sliding Wear Test

After getting the physical and mechanical properties of the composite materials, tribological behavior was investigated using sliding wear test set up. Wear test was conducted using a pin on disc tribometer machine (model TR20, Ducom, Bangalore, India) in the ambient atmosphere (relative humidity $45 \pm 10\%$ and ambient temperature $25 \pm 5^\circ\text{C}$). The schematic of pin on disc wear test set up is shown in Fig. 2. Pin was made of fabricated composite material

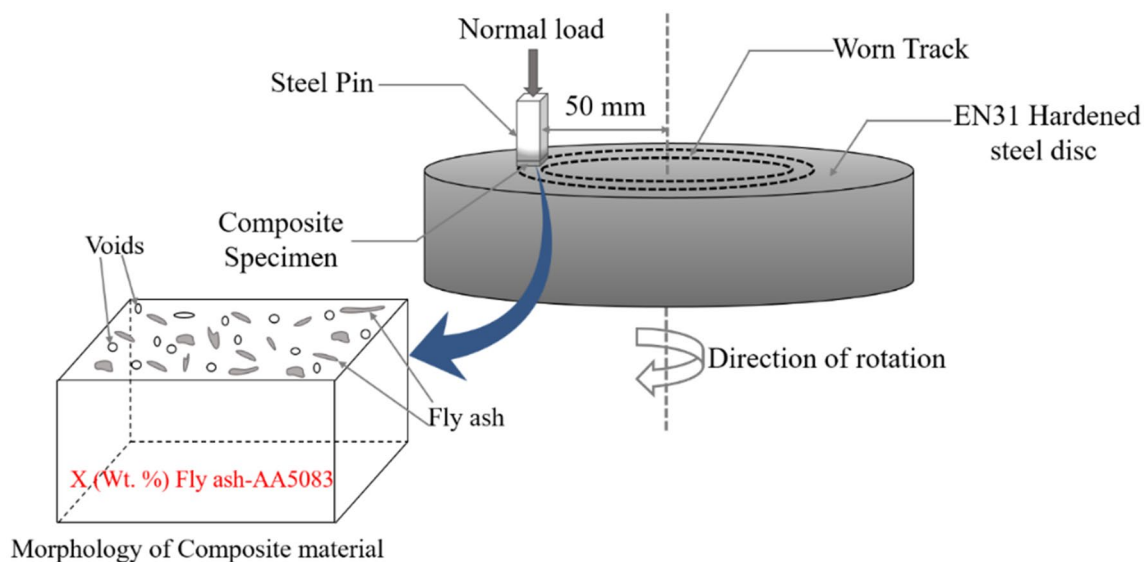


Fig. 2 Schematic of pin on disc sliding wear test set up

Table 2 Different controlling factors and levels used in the wear test

Controlling factors	Levels			Units
	1	2	3	
Sliding velocity (A)	1.047	2.094	3.140	(m/s)
Filler content (B)	0	4	8	(%)
Normal load (C)	5	15	25	(N)

with dimensions $8 \times 8 \times 4 \text{ mm}^3$, which slid against EN31 hardened steel counterbody (having hardness 60–70 HRC). During wear test, traveling circle diameter and the sliding distance were fixed as 50 mm and 1000 m, respectively. Sliding velocity was varied as 1.047 m/s, 2.094 m/s, and 3.140 m/s. Apart from sliding velocity, applied normal load was also varied with values 5, 15, and 25 N to examine the effect of load on wear behavior. The experimental parameters are shown in detail in Table 2 with different levels where each level indicates a particular experimental condition having a combination of different process parameters. The entire test was carried out at least three times for getting repeatability and reproducibility in wear data. After completion of wear test, wear volume was calculated in terms of weight loss using precision electronic balance having accuracy $\pm 0.001 \text{ g}$. Also, the specific wear rate ($\text{mm}^3/\text{N}\cdot\text{m}$) was calculated by the following equation [27]:

$$\text{Specific wear rate } (W_s) = \frac{\Delta M}{\rho_t \cdot V_s \cdot t \cdot F_n} \quad (4)$$

where ΔM is weight loss of composite (g), which is the difference of weight of composite before wear test (M_1) and weight of composite after wear test (M_2), ρ_t is the theoretical density of composites (g/cm^3), V_s is sliding velocity (m/s), F_n is normal load (N), and t is test duration (s).

After the wear test, the worn surface morphology of samples was examined using scanning electron microscopy (SEM) to find out the wear mechanism. The chemical composition of the worn surfaces was examined using energy dispersive spectroscopy (EDS) analysis.

2.5 Experimental Design

Taguchi method was used as a design tool to optimize the outcomes in terms of multiple input variables and responses. This technique helps in solving complex problems to restrict the experimental runs without considerable loss of data. In the present technique, signal-to-noise (S/N) ratio was used as the performance characteristic of fabricated composites. Three different categories of S/N ratio are generally used to optimize the process parameter, viz., larger-the-better model, smaller-the-better model, and nominal-the-better

Table 3 Theoretical L9 orthogonal table using Taguchi method

Control factor/ Experiment number	A	B	C
1	1	1	1
2	1	2	2
3	1	3	3
4	2	1	2
5	2	2	3
6	2	3	1
7	3	1	3
8	3	2	1
9	3	3	2

model. For tribological characterization, smaller-is-better or lower-is-better approach was implemented for investigating the wear rate of fly ash reinforced composite. Since three input parameters, i.e., filler content, sliding velocity, and normal load were used, therefore, L9 orthogonal array design (Table 3) was used for particular output such as specific wear rate. The S/N ratio with lower-is-better performance characteristic can be expressed as:

$$\frac{S}{N} = -10 \log \frac{1}{n} \left(\sum y^2 \right) \quad (5)$$

where n is number of observations, and y is the observed data.

Generally, the experimental design method requires a large number of sample points for several process parameters. Taguchi method can be used as a simple and effective tool for process parameter selection along with experiment planning to reduce the number of trials. In this method, the largest value of signal-to-noise (S/N) ratio is necessary while analyzing the response using signal-to-noise (S/N) ratio. After completion of the experiment, design data were analyzed to determine the optimum levels of controlling factors and confirmation of results.

3 Results and Discussion

3.1 Physical Properties of Composite

3.1.1 Effect of Reinforcement on Density and Void Fraction

The calculated values of theoretical and experimental density of fabricated composites are shown in Fig. 3. We observe that magnitude of experimental density remains comparatively lower than that of theoretical density. The fabricated composites show lower density than that of AA5083 alloy, and it keeps on decreasing with an increase in the fly ash content. These two kinds of densities were used in

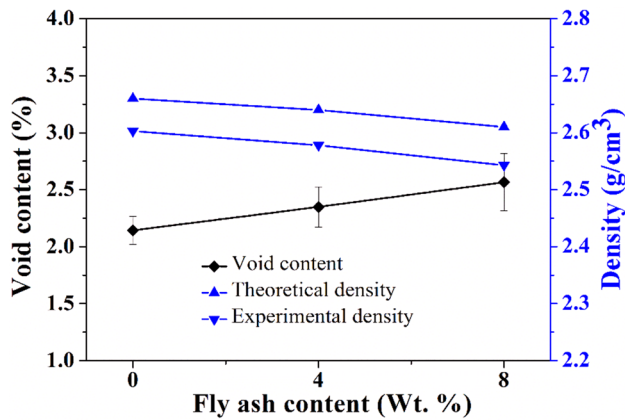


Fig. 3 Variation of void content and density with varying fraction of fly ash in AA5083 alloy-based composite

calculating void fraction as per Eq. (1). It can be observed from Fig. 3 that with an increase in reinforcement content, the void fraction of composites increases, and the maximum void fraction is obtained for 8 wt.% reinforcement. The reason for this may be the agglomeration of fly ash particulates, which increases on increasing the fly ash content and not able to spread uniformly during the stir casting process. It might also form due to the gas entrapment during the stirring process and the formation of air bubbles at the time of

mixing the fly ash particulates with the molten Al matrix during the fabrication process [28, 29].

3.1.2 Surface Morphology of Composites

Surface morphology of fabricated composites was examined using SEM to observe the initial condition, i.e., the effect of void content. It is shown in Fig. 4a-c for varying fractions of fly ash. It can be observed that the composite surface for 0 wt.% fly ash content is quite smooth. With an increase in fly ash content (i.e., for 4 and 8 wt.% fly ash), the composite surface becomes rough and contains fine pores, as visible from the larger magnification image shown in the inset. The increase in void fraction with an increase in fly ash content causes these fine pores. Apart from the fine pores, cracks were also detected, which might have formed due to residual compressive and thermal stresses developed during the stir casting process.

3.2 Mechanical Properties of Composite

3.2.1 Effect of Reinforcement on Hardness

Hardness of fly ash reinforced composite was evaluated experimentally and shown in Fig. 5. Since the hardness of

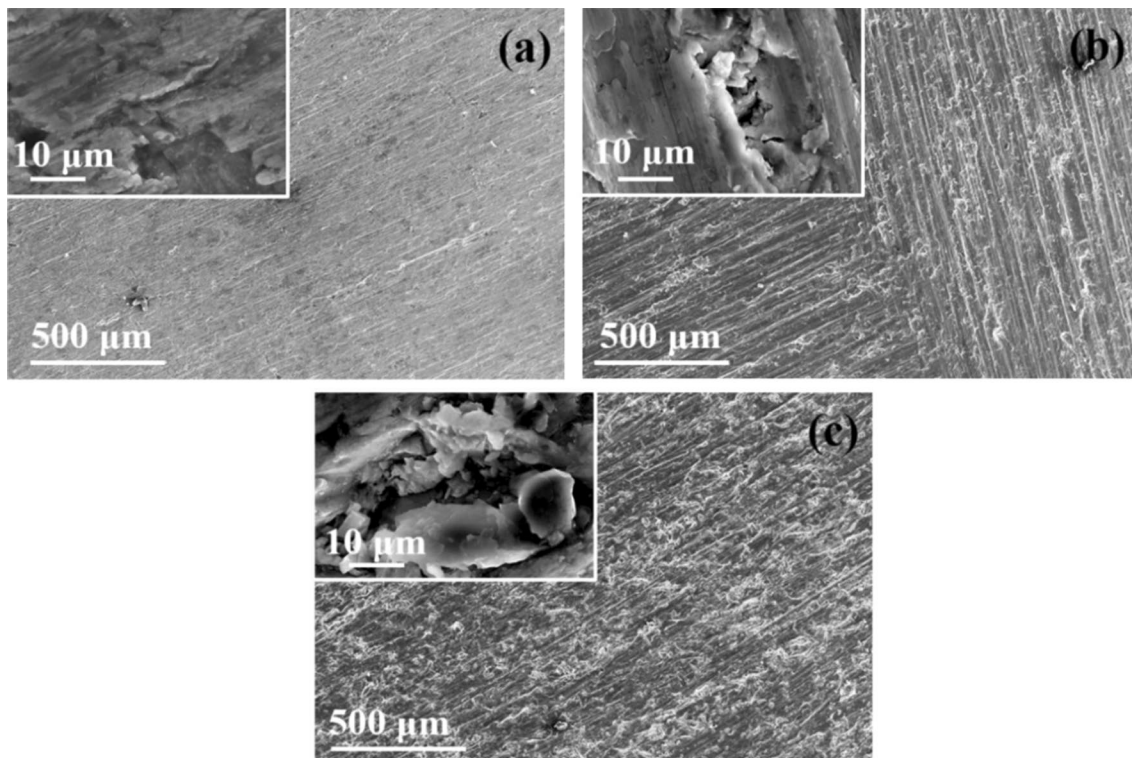


Fig. 4 Surface morphology of fabricated AA5083 alloy-based composites for **a** 0 wt.% **b** 4 wt.%, and **c** 8 wt.% fly ash content

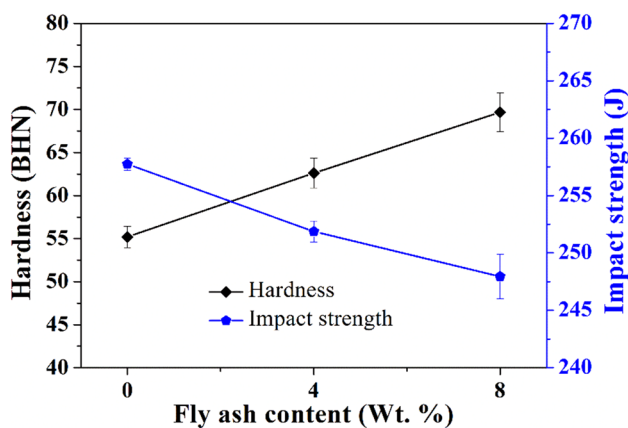


Fig. 5 Variation of hardness and impact strength with varying fraction of fly ash in AA5083 alloy-based composite

fly ash is more than that of base AA5083 alloy, therefore, hardness of fabricated composite increases linearly with an increase in the fraction of fly ash. We obtained maximum hardness, i.e., ~70 BHN for 8 wt.% fly ash reinforced composite, which is ~28% more than that of 0 wt.% fly ash reinforced composite (~54.7 BHN). The reason for this increase in hardness with an increase in fly ash content may be a large amount of dislocations generation due to the incorporation of fine particles. An increase in the hardness of the composite with the incorporation of hard dispersoids has been observed by various researchers [30–32].

3.2.2 Effect of Reinforcement on Impact Strength

After examining the hardness of the fabricated composite, impact strength was tested using the Charpy impact test. Impact strength of fly ash reinforced composite is shown in Fig. 5. It can be observed that impact strength decreases with

an increase in the fraction of fly ash. The increase in void fraction (with the increase in fly ash content) causes a reduction in the interfacial bonding between AA5083 alloy matrix and reinforced particulates, which directly affects the impact strength of the fabricated composite. Also, the increased fly ash content as reinforcement acts as barriers to dislocation movement in the matrix, resulting in an increase in the number of local stress concentration sites, which causes an embrittlement effect in the composite.

3.3 Tribological Properties of Composite

Wear is the gradual loss of the material from the surface when there is a mechanical interaction between the surfaces. Once a soft material (pin) has relative sliding motion against hard counterbody (disc) under applied load, soft material gets worn out, and the process is known as sliding wear [33]. Materials with a low wear rate can improve machine efficiency by maintaining the design tolerance of the components for a longer time duration. Therefore, hard phase reinforced composite was used as initial material for automotive engine pistons applications because it results in increased power output along with better component life. Process parameters like sliding velocity and normal load largely affect the properties of material during the wear process and alter the efficiency of the component along with component life. So, in order to understand the effect of process parameters, a detailed analysis was performed, as explained below.

3.3.1 Effect of Sliding Velocity on Tribological Behavior

Sliding velocity is a prominent process parameter that largely affects the wear performance of machine components in commercial applications. Therefore, wear test was

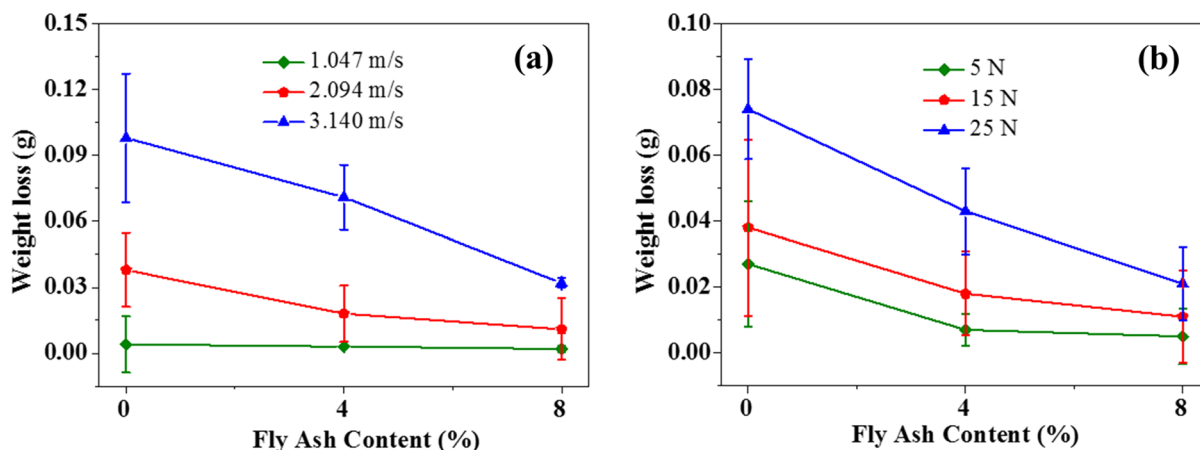


Fig. 6 Variation of weight loss with fraction of reinforcement for different a sliding velocities at constant load (15 N) and b normal loads at constant sliding velocity (2.094 m/s)

conducted to evaluate the influence of sliding velocity on fly ash reinforced composite at constant load of 15 N. In order to calculate weight loss, weight of composites before and after wear test was measured. Difference in weight before and after wear test is illustrated in Fig. 6a. It can be observed that an increase in the fly ash content at constant sliding velocity results in a decrease in the weight loss of the composites. A significant drop in weight loss was observed at the largest sliding velocity (3.14 m/s) from 0 wt.% to 8 wt.% fly ash content.

Similarly, the specific wear rate of fly ash reinforced composite was also investigated, which is shown in Fig. 7a. Specific wear rate can be observed to decrease with an increase in fly ash content and with a decrease in sliding velocity. There is a significant fluctuation in the specific wear rate from $\sim 817 \times 10^{-8} \text{ mm}^3/\text{N}\cdot\text{m}$ (for 3.14 m/s) to $\sim 100 \times 10^{-8} \text{ mm}^3/\text{N}\cdot\text{m}$ (1.047 m/s) on varying sliding velocity for 0 wt.% fly ash content. However, the wear rate decreases substantially after increasing the fraction of fly ash content by 4 wt.% and 8 wt.%. The decrease in wear rate is due to increased hardness of composite on varying the fraction of fly ash.

3.3.2 Effect of Normal Load on Tribological Behavior

Besides sliding velocity, normal load is another important process parameter that generally affects the wear performance. Therefore, wear test was also performed with varying normal load keeping constant sliding velocity 2.094 m/s to investigate the influence of load on weight loss and wear rate. Wear volume in terms of weight loss with varying load was calculated and shown in Fig. 6b. Drop in weight loss of composite was found with an increase in the fraction of reinforcement. Also, weight loss increases after increasing the normal load from 5 to 25 N at constant filler content.

The largest drop in weight loss ($\sim 92\%$) was observed for the lowest load (5 N) followed by $\sim 72\%$ drop in weight loss for 15 N load and again $\sim 72\%$ drop in weight loss for 25 N load. A high drop in weight loss in 8 wt.% fly ash content is due to the presence of a larger fraction of hard phase reinforcement.

The effect of normal load (i.e., 5 N, 15 N, and 25 N) on the specific wear rate of fly ash reinforced composite was also calculated and shown in Fig. 7b. It can be observed that the wear rate decreases continuously by increasing the fraction of fly ash in the composite at a constant load. It is also observed that the largest fly ash (8 wt.%) contained composite is not much affected by the normal load in comparison to the lower fly ash contained composite.

After comparing the experimental results of specific wear rate for different composites, we obtain the lowest specific wear rate for sliding velocity 1.05 m/s, fly ash content 8 wt.%, and normal load 15 N applied during wear test.

3.3.3 Worn Surface Morphology

After investigating the wear behavior of fabricated composite materials, the worn surface morphology of wear sample was explored in SEM in back-scattered electron (BSE) mode to find the wear mechanism and correlate it with wear properties. The surface morphology of worn surface in the fabricated composites with varying fraction of fly ash, i.e., 0 wt.%, 4 wt.%, and 8 wt.% at constant load 15 N and sliding distance 1000 m is demonstrated in Fig. 8a–c. Figure 8a clearly shows that sliding motion of composite pin (0 wt.% fly ash) against hard counterbody leads to the formation of wider and deeper severe abrasive grooves along with brittle type fracture in the grooves. Breakage of materials in the abrasive groove is clearly shown in the inset of Fig. 8a at larger magnification. The absence of fly ash in the composite leads to lower hardness compared to the composite

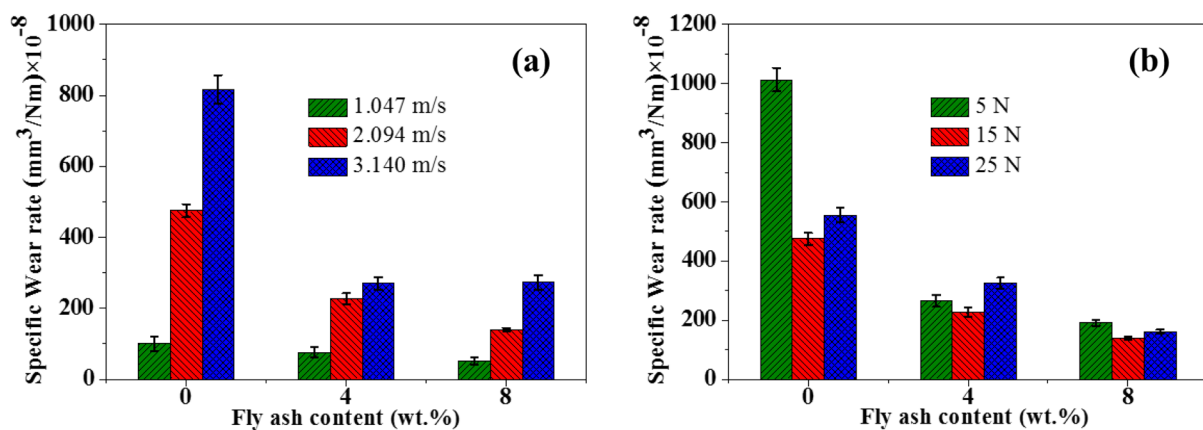


Fig. 7 Variation of wear rate with respect to fly ash content with varying **a** sliding velocities at constant load (15 N) and **b** normal loads at constant sliding velocity (2.094 m/s) for fabricated composites

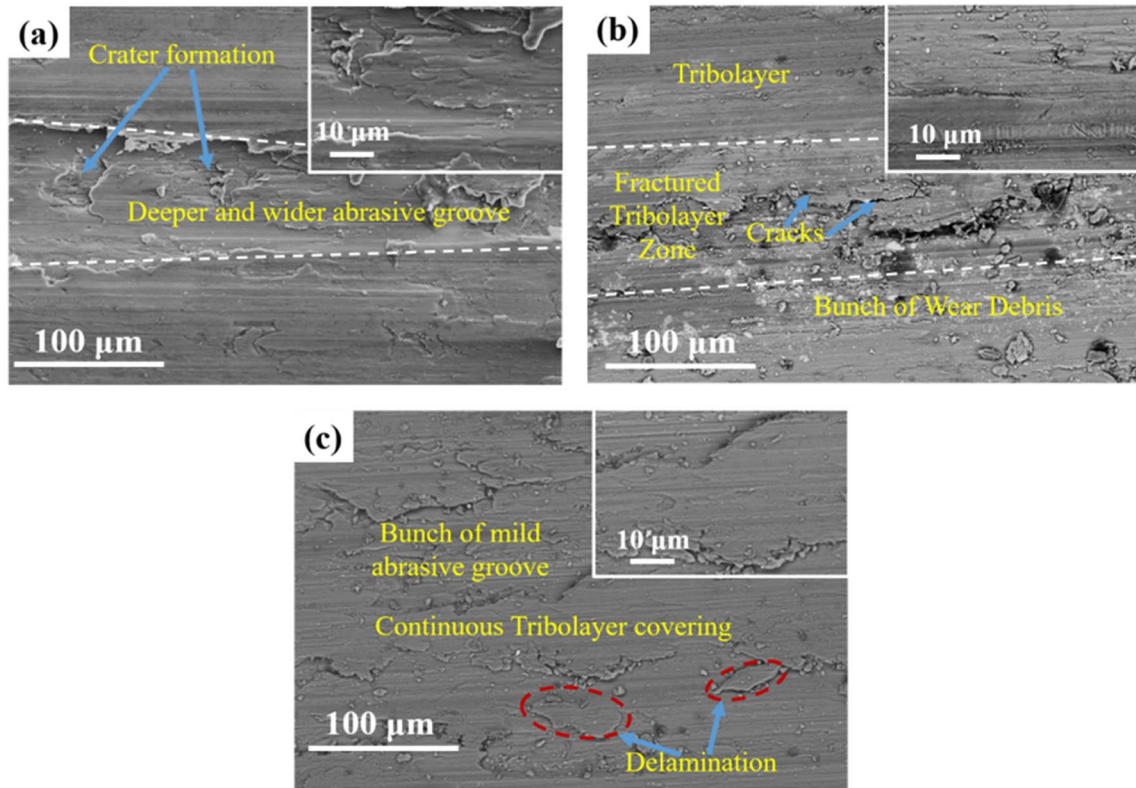


Fig. 8 Worn surface morphology of **a** 0 wt.% **b** 4 wt.% and **c** 8 wt.% fly ash reinforced AA5083 alloy-based composites subjected to wear test at constant load 15 N and sliding distance 1000 m

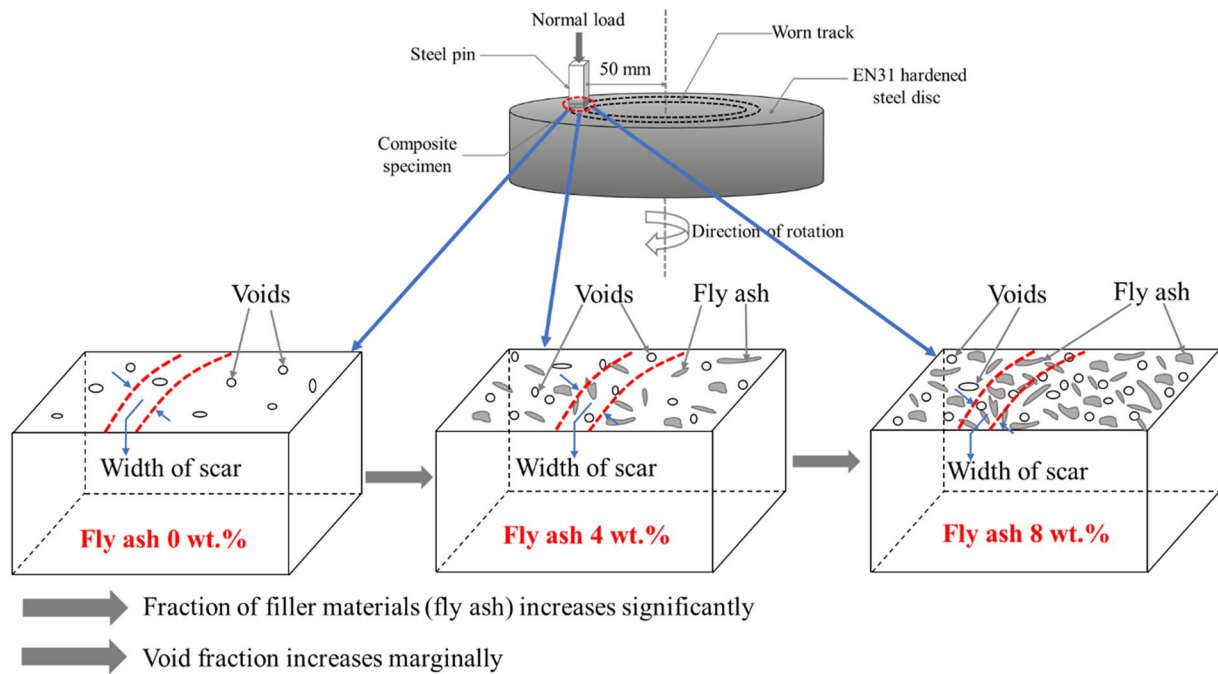


Fig. 9 Schematic of fracture mechanism involved in wear test of 0 wt.%, 4 wt.%, and 8 wt.% fly ash reinforced AA5083 alloy-based composite

having a larger fraction of fly ash and results in the formation of deeper abrasive groove, which is explained through the schematic of wear mechanism shown in Fig. 9. From the schematic, it can be understood when there is no fly ash content, only voids along with AA5083 alloy matrix come in direct contact with hard counterbody during wear test. So, this material becomes more susceptible to the formation of severe abrasion grooves. After increasing the fraction of fly ash to 4 wt.%, the fraction of hard phase increases, as shown in Fig. 9. When composite pin slides against steel disc, some portion of composite pin where fly ash comes in direct contact with steel counterbody leads to lower down the weight loss. Hence, the depth and width of abrasive grooves decreases, as observed from Fig. 8b. The remaining portion of composite with an absence of fly ash gets worn out, similarly to 0 wt.% fly ash reinforced composite.

Further, an increase in fly ash content up to 8 wt.% causes a high increase in the hardness and results in significant improvement of wear resistance and leads to the very low depth of abrasive grooves, as observed from Fig. 8c. This composition shows a comparatively larger portion of

the surface covered with fly ash, as shown schematically in Fig. 9. Therefore, the material removal rate reduces, and a portion of composite, where wear debris comes out, starts protecting the composite pin with the formation of a dense oxide layer. With the passage of time, the ability of the protective layer to further protect the surface decreases because of the fragmentation of tribolayer into small pieces. These small pieces of oxide act as a third body, which generates very mild abrasive grooves due to the third body abrasion mechanism [34]. The fragmentation of the oxide layer causes delamination, as shown in Fig. 8c. The increase in pin-disc interface temperature during sliding wear test leads to the removal of hard fly ash particles from the fabricated composite, which also causes the delamination of the surface.

Now, to examine the composition of the protective oxide layer, energy dispersive spectroscopy (EDS) analysis was done for all the composites, which is shown in Fig. 10a–c. From EDS spectra, it is clear that the fraction of oxygen increases in composite materials with increasing the fraction of fly ash content, which leads to the formation of the protective oxide layer. Since aluminum and magnesium both

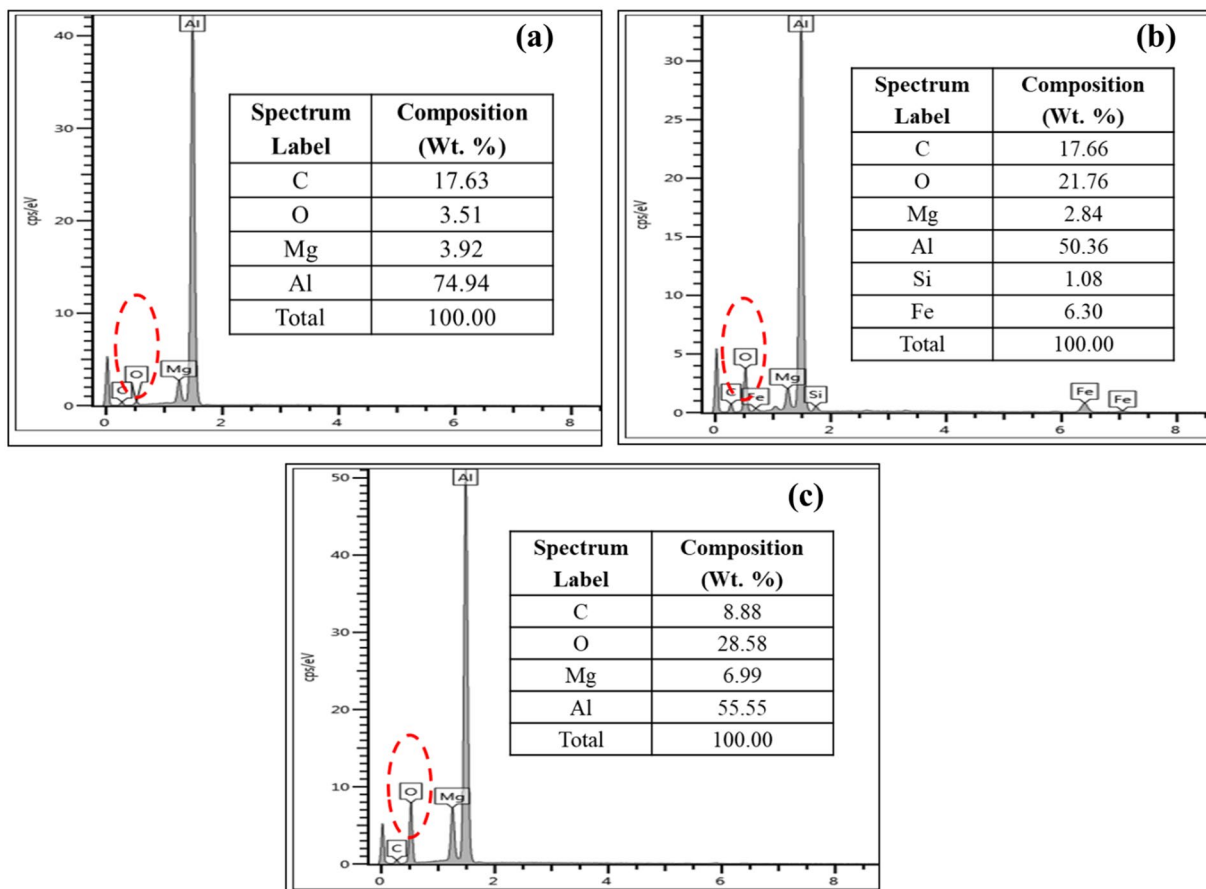


Fig. 10 Worn surface morphology of **a** 0 wt.% **b** 4 wt.%, and **c** 8 wt.% fly ash reinforced AA5083 alloy-based composites subjected to wear test at constant load 15 N and sliding distance 1000 m

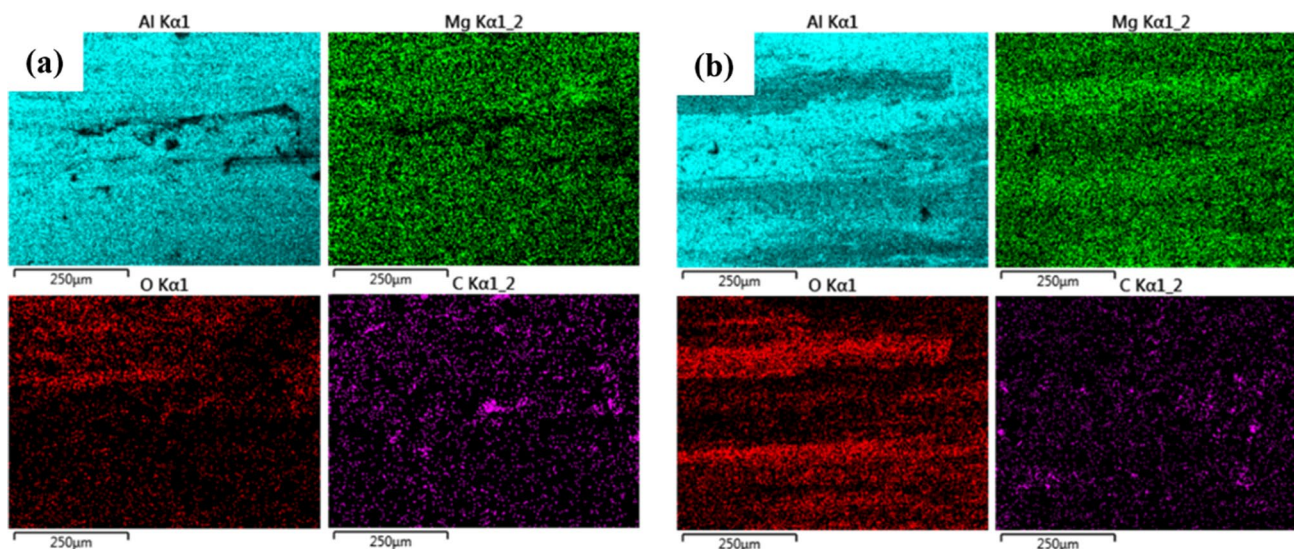


Fig. 11 Elemental mapping of worn surface of **a** 0 wt.% and **b** 8 wt.% fly ash reinforced AA5083 alloy-based composites subjected to wear test at constant load 15 N and sliding distance 1000 m

are prone to make oxide in an ambient atmosphere, therefore, the protective oxide layer may be a combination of aluminum and magnesium oxide. Consequently, to understand the distribution of different protective oxide layer in terms of the exact distribution of oxygen and other alloying elements of composite, elemental mapping was performed using SEM–EDS, which is shown in Fig. 11a and b for 0 wt.% and 8 wt.% composite material, respectively. It can be observed that, for 0 wt.% fly ash reinforced composite, all the elements excluding oxygen are uniformly distributed, and the fraction of oxygen is very less (Fig. 11b). Composite having a larger fraction of fly ash (8 wt.%) contains a significant amount of oxygen (Fig. 11b). This larger fraction of oxygen leads to the formation of either aluminum oxide, magnesium oxide or a combination of both as some portions of mapping are observed to enrich in oxygen-magnesium combination while others are enriched in oxygen-aluminum combination.

3.3.4 Optimization of Wear Rate Using Taguchi Method

After completion of the wear test of fly ash reinforced composites, optimized (best suited) process parameters were examined for obtaining the minimum wear rate among all the sample conditions. Taguchi design of experiments (DOE) approach was used to understand the correlation of specific wear rate with controlling variables (3 in the present study) used for the wear test. For implementing the Taguchi DOE approach, we established the ranking order of controlling variables, which is shown in Table 3. Here, three controlling variables were used, which results in an L9 orthogonal array. The L9 orthogonal array of runs for the obtained experimental results is tabulated in Table 4. Signal to noise ratio (S/N ratio) for each experimental run was calculated using commercially available MINITAB 16 software for smaller-the-better value because the smaller value of specific wear rate is the most desirable. Wear rate corresponding to the larger signal-to-noise ratio was eliminated.

To obtain the optimized value from different conditions, higher S/N ratio was selected from Table 4. The main effect plot for different materials with several process parameters

Table 4 Experimental layout of L9 orthogonal array

Serial number	1	2	3	4	5	6	7	8	9
Sliding velocity (m/s)	1.047	1.047	1.047	2.094	2.094	2.094	3.14	3.14	3.14
Filler content (%)	0	4	8	0	4	8	0	4	8
Load (N)	5	15	25	15	25	5	25	5	15
Wear rate (mm ³ /N-m) × 10 ⁻⁸	75	25.21	38.29	475.01	325.33	459.36	37.51	113.52	25.52
S/N ratio (dB)	-37.5	-28.03	-31.66	-53.53	-50.25	-53.24	-31.48	-41.1	-28.14

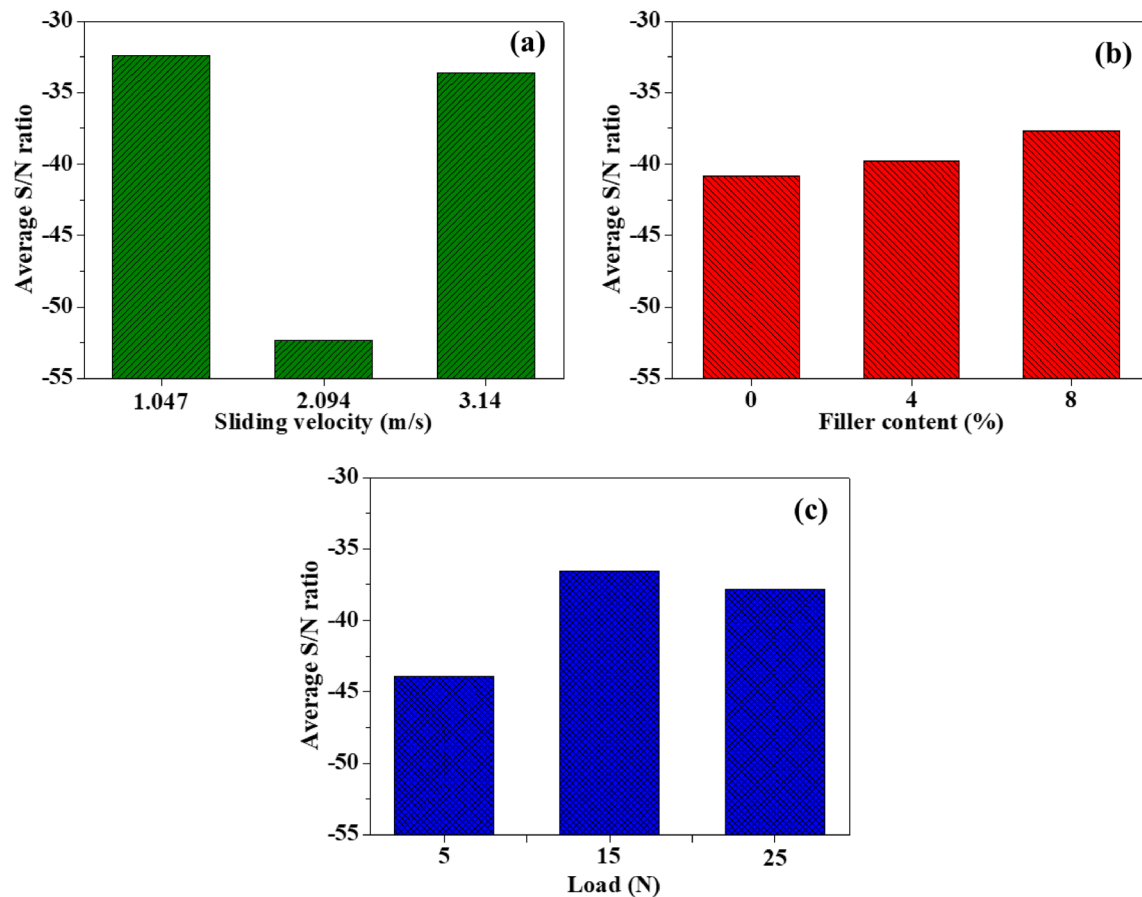


Fig. 12 Main effects plot for S/N ratio for different controlling factors of wear rate for fly ash reinforced AA5083 alloy-based composite **a** sliding velocity, **b** filler content, and **c** load

is shown in Fig. 12. This figure clearly shows that 1.047 m/s sliding velocity, 8 wt.% fly ash, and 15 N load is the best combination of process parameters among the entire selected factors to obtain the required outcome of fly ash reinforced AA5083 alloy-based composite materials in the present study.

4 Summary and Conclusions

In the current work, AA5083 aluminum alloy-based metal matrix composites were fabricated using high temperature vacuum stir casting technique with varying fraction of fly ash as reinforcement viz. 0 wt.%, 4 wt.%, and 8 wt.%. The fabricated composites were comparatively studied in terms of their physical, mechanical, and tribological properties. Fly ash is a waste byproduct produced during the combustion of coal and hazardous to the environment. Their utilization as reinforcement in metal matrix composite is expected to result in low cost, environment-friendly, and enhanced

performance of the material. The pertinent conclusions drawn from the present study are given below.

1. As density of fly ash is lower than that of AA5083 alloy, increasing the fraction of reinforcement results in a decrease in the overall density of the composite. It leads to the formation of voids, and so, the fraction of voids increases with increasing fly ash content.
2. There is a continuous increase in the hardness of composites with an increase in the fraction of fly ash. Approximately 28% increase in hardness was observed for 8 wt.% fly ash reinforced composite in comparison to that of 0 wt.% fly ash AA5083 alloy.
3. There is a continuous decrease in impact strength with an increase in reinforcement fraction, however, it is only a marginal decrease. Impact strength of 8 wt.% fly ash reinforced AA5083 composite decreases by ~3.8% in comparison to that of 0 wt.% fly ash reinforced composite.

4. Wear resistance of composite improves with increasing fly ash content for an increase in both sliding velocity and normal load. Also, significant fluctuation in wear rate from $\sim 817 \times 10^{-8} \text{ mm}^3/\text{N}\cdot\text{m}$ (for 3.14 m/s) to $\sim 100 \times 10^{-8} \text{ mm}^3/\text{N}\cdot\text{m}$ (1.047 m/s) was observed on varying sliding velocity for 0 wt.% fly ash content. This perturbation in wear rate decreases substantially for a larger fraction of fly ash (8 wt.%), which indicates that 8 wt.% reinforced composite has the best tribological characteristics among all the fabricated composites.
5. After comparing the overall results using Taguchi DOE approach, the minimum wear rate was obtained for sliding velocity 1.047 m/s, fly ash content 8 wt.%, and normal load 15 N.

Acknowledgements The authors gratefully acknowledge the Advanced Research Centre for Tribology, Malaviya National Institute of Technology, Jaipur, India, for providing wear test facility used in the current work.

Authors' Contributions Swati Gangwar: Conceptualization, Methodology, Visualization, Formal analysis, Data curation, Investigation, Supervision, Writing—review & editing. Ranjeet Kumar Singh: Conceptualization, Methodology, Formal analysis, Data curation, Investigation, Writing original draft. Prabhat Chand Yadav: Visualization, Writing original draft. Sandeep Sahu: Visualization, Formal analysis, Writing original draft, Writing—review & editing.

Funding The author(s) received no financial support for the research, authorship, and/or publication of this article.

Data Availability The data that support the findings of this study are available from the corresponding author, Swati Gangwar, upon reasonable request.

Declarations

Conflict of interest The author(s) declared no potential conflicts of interest with respect to the research, authorship, and/or publication of this article.

References

1. Miller WS, Zhuang L, Bottema J, Wittebrood AJ, De Smet P, Haszler A, Vieregge A (2000) Recent development in aluminium alloys for the automotive industry. *Mater Sci Eng, A* 280:37–49. [https://doi.org/10.1016/S0921-5093\(99\)00653-X](https://doi.org/10.1016/S0921-5093(99)00653-X)
2. Prasad SV, Asthana R (2004) Aluminum metal-matrix composites for automotive applications: tribological considerations. *Tribol Lett* 17:445–453. <https://doi.org/10.1023/B:TRIL.0000044492.91991.f3>
3. Rajmohan T, Palanikumar K, Ranganathan S (2013) Evaluation of mechanical and wear properties of hybrid aluminium matrix composites. *Trans Nonferrous Met Soc China* 23:2509–2517. [https://doi.org/10.1016/S1003-6326\(13\)62762-4](https://doi.org/10.1016/S1003-6326(13)62762-4)
4. Lindroos VK, Talvitie MJ (1995) Recent advances in metal matrix composites. *J Mater Process Technol* 53:273–284. [https://doi.org/10.1016/0924-0136\(95\)01985-N](https://doi.org/10.1016/0924-0136(95)01985-N)
5. Cheriaf M, Rocha JC, Péra J (1999) Pozzolanic properties of pulverized coal combustion bottom ash. *Cem Concr Res* 29:1387–1391. [https://doi.org/10.1016/S0008-8846\(99\)00098-8](https://doi.org/10.1016/S0008-8846(99)00098-8)
6. Sharma SK, Kalra N (2006) Effect of flyash incorporation on soil properties and productivity of crops: A review. *J Sci Ind Res* 65:383–390
7. Martinello K, Oliveira MLS, Molossi FA, Ramos CG, Teixeira EC, Kautzmann RM, Silva LFO (2014) Direct identification of hazardous elements in ultra-fine and nanominerals from coal fly ash produced during diesel co-firing. *Sci Total Environ* 470–471:444–452. <https://doi.org/10.1016/j.scitotenv.2013.10.007>
8. Silva LFO, DaBoit K, Sampaio CH, Jasper A, Andrade ML, Kostova IJ, Waanders FB, Henke KR, Hower JC (2012) The occurrence of hazardous volatile elements and nanoparticles in Bulgarian coal fly ashes and the effect on human health exposure. *Sci Total Environ* 416:513–526. <https://doi.org/10.1016/j.scitotenv.2011.11.012>
9. Anilkumar HC, Hebbar HS, Ravishankar KS (2011) Mechanical properties of fly ash reinforced aluminium alloy (Al6061) composites. *Int J Mech Mater Eng* 6:41–45
10. Rohatgi PK, Kim JK, Gupta N, Alaraj S, Daoud A (2006) Compressive characteristics of A356/fly ash cenosphere composites synthesized by pressure infiltration technique. *Compos Part A Appl Sci Manuf* 37:430–437. <https://doi.org/10.1016/j.compositesa.2005.05.047>
11. Juang SH, Xue C-S (2015) Investigation of mechanical properties and microstructures of aluminum-fly ash composite processed by friction stirring. *Mater Sci Eng, A* 640:314–319. <https://doi.org/10.1016/j.msea.2015.06.015>
12. Sudarshan SMK (2008) Synthesis of fly ash particle reinforced A356 Al composites and their characterization. *Mater Sci Eng, A* 480:117–124. <https://doi.org/10.1016/j.msea.2007.06.068>
13. Rao JB, Rao DV, Murthy IN, Bhargava N (2012) Mechanical properties and corrosion behaviour of fly ash particles reinforced AA 2024 composites. *J Compos Mater* 46:1393–1404. <https://doi.org/10.1177/0021998311419876>
14. Mohammed Razzaq A, Majid DL, Ishak MR, Basheer UM (2017) Effect of fly ash addition on the physical and mechanical properties of AA6063 alloy reinforcement. *Metals* 7:477. <https://doi.org/10.3390/met7110477>
15. David Raja Selvam J, Robinson Smart DS, Dinaharan I (2013) Microstructure and some mechanical properties of fly ash particulate reinforced AA6061 aluminum alloy composites prepared by compocasting. *Mater Des* 49:28–34. <https://doi.org/10.1016/j.matdes.2013.01.053>
16. El-Khair MA, Lotfy A, Daoud A, El-Sheikh A (2011) Microstructure, thermal behavior and mechanical properties of squeeze cast SiC, ZrO₂ or C reinforced ZA27 composites. *Mater Sci Eng, A* 528:2353–2362. <https://doi.org/10.1016/j.msea.2010.11.060>
17. Patil MSR, Motgi B (2013) A study on mechanical properties of fly ash and alumina reinforced aluminium alloy (LM25) composites. *IOSR-JMCE* 7:41–46. <https://doi.org/10.9790/1684-0764146>
18. Ramachandra M, Radhakrishna K (2007) Effect of reinforcement of flyash on sliding wear, slurry erosive wear and corrosive behavior of aluminium matrix composite. *Wear* 262:1450–1462. <https://doi.org/10.1016/j.wear.2007.01.026>
19. Sudarshan SMK (2008) Dry sliding wear of fly ash particle reinforced A356 Al composites. *Wear* 265:349–360. <https://doi.org/10.1016/j.wear.2007.11.009>
20. Venkat Prasat S, Subramanian R (2013) Tribological properties of AISi10Mg/fly ash/graphite hybrid metal matrix

- composites. *Ind Lubr Tribol* 65:399–408. <https://doi.org/10.1108/ILT-05-2011-0031>
21. Uthayakumar M, Kumaran ST, Aravindan S (2013) Dry sliding friction and wear studies of fly ash reinforced AA-6351 metal matrix composites. *Adv Tribol*. <https://doi.org/10.1155/2013/365602>
 22. Dinaharan I, Nelson R, Vijay SJ, Akinlabi ET (2016) Microstructure and wear characterization of aluminum matrix composites reinforced with industrial waste fly ash particulates synthesized by friction stir processing. *Mater Charact* 118:149–158. <https://doi.org/10.1016/j.matchar.2016.05.017>
 23. Hatch JE (1984) *Aluminum: Properties and Physical Metallurgy*. OH, American Society for Metals, Metals Park
 24. Rohatgi P (1991) Cast aluminum-matrix composites for automotive applications. *JOM* 43:10–15. <https://doi.org/10.1007/BF03220538>
 25. Wu GH, Dou ZY, Jiang LT, Cao JH (2006) Damping properties of aluminum matrix–fly ash composites. *Mater Lett* 60:2945–2948. <https://doi.org/10.1016/j.matlet.2006.02.018>
 26. Agarwal B, Broutman L (1990) *Analysis and Performance of Fiber Composites*, 2nd edn. John Wiley & Sons, New York
 27. Verma R, Srinivasan A, Jayaganthan R, Nath SK, Goel S (2017) Studies on tensile behaviour and microstructural evolution of UFG Mg-4Zn-4Gd alloy processed through hot rolling. *Mater Sci Eng, A* 704:412–426. <https://doi.org/10.1016/j.msea.2017.08.032>
 28. Kok M (2005) Production and mechanical properties of Al₂O₃ particle-reinforced 2024 aluminium alloy composites. *J Mater Process Technol* 161:381–387. <https://doi.org/10.1016/j.jmatp.rotec.2004.07.068>
 29. Lee CJ, Huang JC, Hsieh PJ (2006) Mg based nano-composites fabricated by friction stir processing. *Scr Mater* 54:1415–1420. <https://doi.org/10.1016/j.scriptamat.2005.11.056>
 30. Poddar P, Mukherjee S, Sahoo K (2009) The microstructure and mechanical properties of SiC reinforced magnesium based composites by rheocasting process. *J Mater Eng Perform* 18:849–855. <https://doi.org/10.1007/s11665-008-9334-1>
 31. Yang H, Topping TD, Wehage K, Jiang L, Lavernia EJ, Schoenung JM (2014) Tensile behavior and strengthening mechanisms in a submicron B₄C-reinforced Al trimodal composite. *Mater Sci Eng, A* 616:35–43. <https://doi.org/10.1016/j.msea.2014.07.079>
 32. Yang H, Jiang L, Balog M, Krizik P, Schoenung JM (2017) Reinforcement size dependence of load bearing capacity in ultrafine-grained metal matrix composites. *Metall Mater Trans A* 48:4385–4392. <https://doi.org/10.1007/s11661-017-4186-7>
 33. Deuis R, Subramanian C, Yellup J (1997) Dry sliding wear of aluminium composites—a review. *Compos Sci Technol* 57:415–435. [https://doi.org/10.1016/S0266-3538\(96\)00167-4](https://doi.org/10.1016/S0266-3538(96)00167-4)
 34. Gates J (1998) Two-body and three-body abrasion: a critical discussion. *Wear* 214:139–146. [https://doi.org/10.1016/S0043-1648\(97\)00188-9](https://doi.org/10.1016/S0043-1648(97)00188-9)

Publisher's Note Springer Nature remains neutral with regard to jurisdictional claims in published maps and institutional affiliations.